Research Article | Vol. 9, No. 11 / 1 November 2019 / Optical Materials Express 4399
Optical Materials EXPRESS

Trapping a magnetic rainbow by using a one-way magnetostatic-like mode

Qian Shen,[1,2,3] Linfang Shen,[4,6] Weidong Min,[5] Jie Xu,[2] Chiaho Wu,[4] Xiaohua Deng,[2] and Sanshui Xiao[3,7]

[1]School of Information Engineering, Nanchang University, Nanchang, 330031, China
[2]Institute of Space Science and Technology, Nanchang University, Nanchang, 330031, China
[3]Department of Photonics Engineering, Technical University of Denmark, DK-2800 Kgs. Lyngby, Denmark
[4]Department of Applied Physics, Zhejiang University of Technology, Hangzhou 310023, China
[5]School of Software, Nanchang University, Nanchang, 330031, China
[6]lfshen@zjut.edu.cn
[7]saxi@fotonik.dtu.dk

Abstract: Trapped rainbow effects have been realized in many systems while they are all characterized by electric-field enhancement. The trapped rainbow with strong magnetic-field enhancement has yet to be studied. Here, we achieve the trapped magnetic rainbow effect in a novel metal-air-YIG (yttrium-iron-garnet)-metal (MAYM) waveguide applied with a continuously decreasing magnetic field. The proposed system supports a one-way propagation feature, leading to the suppressed reflection. We systemically analyze the dispersion and the modal properties, showing the transition from the SMP (surface magnetoplasmon)-like mode to magnetostatic-like mode and the change of the group velocity when decreasing the external magnetic field along the propagation direction of the wave. We obtain the trapped magnetic rainbow effects as well as magnetic hotspots both in frequency- and time-domain simulations. The trapped rainbow effect with strong magnetic field enhancement paves a promising way for many applications including magnetic sensing to magnetic non-linearity.

1. Introduction

Magnetostatic waves (MSWs), which are supported by a slab of ferrite material magnetized in the plane of its faces, have been investigated by using magnetostatic approximation [1]. The dispersion characteristics for MSWs in the forward and reverse directions are firstly found to be symmetrical about $k = 0$ [2]. Later it is demonstrated that the symmetry of dispersion can be broken by changing the boundary condition at one face of the ferrite film, such as placing a perfect electric conductor or metamaterial [3–6]. Compared to a air-YIG (yttrium-iron-garnet)-air structure, it is shown that the modes in the air-YIG-metal (AYM) layered structure associated with the air-YIG interface disappear while those modes associated with the metallic surface are modified [3], resulting in the appearance of the non-reciprocal MSWs [4]. But such non-reciprocal MSWs lack robust one-way property and do not have immunity to backscattering, as they can be easily coupled into radiation modes in air through scattering at surface imperfections or bends. On the other hand, MSWs are characterized by very low group velocity. These unique and interesting properties of MSWs provide a promising way for realizing various applications, such as optical communication [7,8], signal processing [8,9] and MSWs based delay line [10]. The one-way MSWs with natural low group velocity can also be used to achieve trapping rainbow. Unfortunately, due to their large wavevector, attention has yet to be paid to achieve the trapped rainbow effect based on MSWs.

Trapping rainbow has attracted significant attentions recently as a potential key for optic data storage, light processing and enhancement of nonlinear effects [11–14]. The purpose of trapping rainbow is to trap different frequency components of incident light or electromagnetic

#377273 https://doi.org/10.1364/OME.9.004399
Journal © 2019 Received 10 Sep 2019; revised 16 Oct 2019; accepted 16 Oct 2019; published 22 Oct 2019

Optical Materials EXPRESS

(EM) waves at different spatial positions [16]. So far, it has been numerically studied in tapered structures such as tapered waveguide based on metamaterial [17,18], tapered photonic crystal waveguides [19], or tapered plasmonic waveguides [20]. It should be mentioned that the incident EM waves in these systems are strongly reflected due to the strong coupling between the forward and backward modes near the critical position [21]. Trapping EM waves without reflection is reported by using one-way surface magnetoplasmons (SMPs) [22–24], however the trapping effect is obtained in a forcible and rapid way by use of a suddenly terminated waveguide, which is not the case for the so-called trapping rainbow effect. By introducing one-way propagating concept [25–27], the trapped rainbow effect is later demonstrated by utilizing one-way SMPs in a metal-air-YIG (MAY) system [28], showing the strong electric-field enhancement, however it remains a big challenge for achieving strong magnetic-field enhancement with many potential applications including magnetic sensing to magnetic non-linearity [29–31].

In this paper, we for the first time demonstrate the rainbow effect with the strong magnetic-field enhancement, which relies on the magnetostatics mode. We firstly propose a novel metal-air-YIG-metal (MAYM) system and analyze the dispersion relation, showing a complete forbidden propagation bandgap as well as a ferromagnetic resonance frequency. The modal properties including the group velocity are further investigated and a threshold frequency is introduced to distinguish the SMP-like modes and magnetostatic-like modes. For our proposed structure, there exists a transition from the SMP-like mode to magnetostatic-like modes by a continuously decreasing H_0 along propagation direction of the wave. We achieve the trapping rainbow effect with strong magnetic field enhancement, which is confirmed both in frequency- and time-domain simulations. Compared to the previous relevant work, we for the first time rely on the magnetostatic-like mode to achieve trapping rainbow instead of using conventional SMPs, thus exhibiting the unique feature of magnetic field enhancement. Our system bridges a gap between EM modes and magnetostatic modes and realizes the magnetic rainbow by using the magnetostatic-like mode.

2. Physical model

We firstly analyze the dispersion properties in the MAYM structure (see the inset in Fig. 1(a)) under a static external magnetic field H_0. The metal herein is assumed to be a perfect electric conductor (PEC), which is a good approximation in the microwave regime. The air layer with relative permittivity ε_r has the thickness of d_1 and the YIG layer with relative permittivity ε_m has the thickness of d_2. Gyromagnetic anisotropy is introduced in the YIG, with the permeability tensor taking the form

$$\overleftrightarrow{\mu}_m = \begin{bmatrix} 1 & 0 & 0 \\ 0 & \mu_1 & i\mu_2 \\ 0 & -i\mu_2 & \mu_1 \end{bmatrix}, \tag{1}$$

with

$$\begin{aligned} \mu_1 &= 1 + \frac{\omega_m(\omega_0 - i\nu\omega)}{(\omega_0 - i\nu\omega)^2 - \omega^2} \\ \mu_2 &= \frac{\omega_m\omega}{(\omega_0 - i\nu\omega)^2 - \omega^2} \end{aligned}, \tag{2}$$

where ω is the angular frequency, $\omega_0 = 2\pi\gamma H_0$ (where γ is the gyromagnetic ratio) is the procession angular frequency, ω_m is the characteristic circular frequency, and ν is the damping coefficient. The fields of guiding modes in the system are transverse-electric-polarized (TE), and

Optical Materials EXPRESS

the nonzero component of the electric field (E_x) can be written as

$$E_x(z,\ y) = [A_1 \exp(-\alpha_r y) + A_2 \exp(\alpha_r y)] \exp[i(kz - \omega t)] \tag{3}$$

in the air layer for $0 \le y \le d_1$, and

$$E_x(z,\ y) = [B_1 \exp(\alpha_m y) + B_2 \exp(-\alpha_m y)] \exp[i(kz - \omega t)] \tag{4}$$

in the YIG layer for $-d_2 \le y<0$, where k is the propagation constant, $\alpha_r = \sqrt{k^2 - \varepsilon_r k_0^2}$ (which is allowed to be real or imaginary) with $k_0 = \omega/c$ (where c is the light speed in vacuum), and $\alpha_m = \sqrt{k^2 - \varepsilon_m \mu_v k_0^2}$ with $\mu_v = \mu_1 - \mu_2^2/\mu_1$ being the Voigt permeability. According to the boundary conditions at the interfaces $y = d_1$, $y = 0$ and $y = -d_2$, we can obtain

$$\alpha_r \mu_v + \left(\frac{\alpha_m}{\tanh \alpha_m d_2} + \frac{\mu_2}{\mu_1} k\right) \tanh(\alpha_r d_1) = 0 \tag{5}$$

Obviously, the guiding modes are nonreciprocal, because there exists a linear term with respect to k in Eq. (5). From Eq. (5) we can find

$$\omega_{sp}^{+} = \omega_0 + \omega_m \tag{6}$$

for $k \to +\infty$, and

$$\omega_{sp}^{-} = \omega_0 + 0.5\omega_m \tag{7}$$

for $k \to -\infty$. ω_{sp}^{+} is associated with the ferromagnetic resonance frequency discussed in the AYM structure [3], which is supported by the interface of the YIG and metal. ω_{sp}^{-} is the plasma resonance frequency of YIG [32], which is supported by the interface of the YIG and air. The dispersion relation in the MAY system can be obtained from Eq. (5) by letting $d_2 \to \infty$, which gives

$$\alpha_r \mu_v + \left(\alpha_m + \frac{\mu_2}{\mu_1} k\right) \tanh(\alpha_r d_1) = 0 \tag{8}$$

Compared to the MAY system, the YIG layer in the present system is terminated by metal slab, thus the bulk modes in the YIG become bound modes, which must satisfy transverse resonance

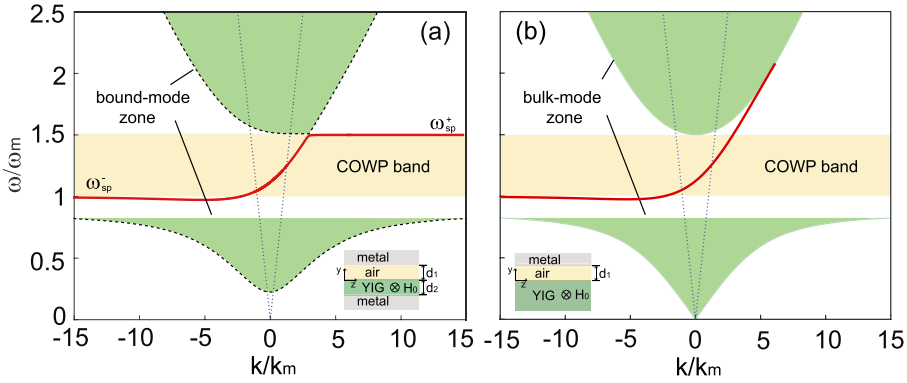

Fig. 1. Dispersion relations in the (a) MAYM and (b) MAY systems. Dashed lines in (a) represent the dispersion curves for bound modes with lowest order in the YIG layer, and green shaded areas in (a) and (b) represent bound-mode and bulk-mode zones respectively. The yellow shaded areas in (a) and (b) represent the complete one-way propagation (COWP) band and dotted lines represent the light line in air. The parameters of the two systems are as follows: $\varepsilon_r = 1$, $\varepsilon_m = 15$; $\omega_0 = 0.5\omega_m$, $\omega_m = 10\pi \times 10^9$ rad/s; $d_1 = 0.05\lambda_m$, $d_2 = 0.3\lambda_m$ and $\nu = 0$.

Optical Materials EXPRESS

condition. Such bound modes, whose properties are closely dependent on the YIG thickness, are guided by a means of zigzag reflections at the metal surface and YIG-air interface, and they are generally allowed to propagate both forward and backward [33].

3. Dispersion and mode analysis

The red line in Fig. 1(a) shows the dispersion relation of the guiding modes for the MAYM system when $d_1 = 0.05\lambda_m$, $d_2 = 0.3\lambda_m$; $\omega_0 = 0.5\omega_m$, $\omega_m = 10\pi \times 10^9$ rad/s. To distinguish guiding mode from evanescent mode (with complex propagation constant), we set $\nu = 0$ in calculating dispersion. The material loss will be taken into account later when we consider wave transmission in the system. For comparison, the dispersion relation of the guiding modes, see the red line, in the equivalent MAY system is plotted in Fig. 1(b). The insets in Figs. 1(a) and 1(b) show schematics of the MAYM and MAY systems, respectively. As discussed before, the guiding modes in the MAYM system are characterized by two resonance frequencies, ω_{sp}^- and ω_{sp}^+. The dispersion curves are similar for $\omega<\omega_{sp}^+$ in these two systems, but rather different for $\omega \geqslant \omega_{sp}^+$. The frequency in the MAY system is monotonously increasing with the wavevector for $k>0$, however, it possesses a resonance frequency in the MAYM system due to the ferromagnetic resonance arising from the finite YIG thickness. Evidently, bulk modes in the YIG for the MAY system are space modes given by $\sqrt{k_z^2 + k_y^2} = \sqrt{\varepsilon_m \mu_v} k_0$ and the bulk-mode zones are illustrated by the green shaded areas in Fig. 1(b). In our proposed MAYM system, bound modes in the YIG are kind of similar to bulk modes, which have the real transverse components (k_y) of wavevectors. The dispersion of the bound modes can be derived from Eq. (5) by letting $k = k_z$, and $\alpha_m = ik_y$ (where k_z and k_y are both real-valued), and it has the form

$$\alpha_r \mu_v + \left(\frac{k_y}{\tan k_y d_2} + \frac{\mu_2}{\mu_1} k \right) \tanh(\alpha_r d_1) = 0 \tag{9}$$

where $\alpha_r = \sqrt{k_z^2 - \varepsilon_r k_0^2}$. Therefore, for a given ω, there only exist discrete solutions, which are associated with the transverse resonances of different orders for the bound mode. The bound mode with the lowest order defining the lowest cutoff of the bound-mode zone is shown in Fig. 1(a) as dashed lines. Compared with the dispersion curve in the AYM system in Ref. 4, the dispersion curves in the MAYM and MAY systems possess a complete one-way propagation (COWP) region indicated by the shaded rectangle areas in Figs. 1(a) and 1(b). As the dispersion curve has a positive slope over the whole COWP region, the guiding mode is only allowed to propagate forward in the MAYM system.

For the case $d_2 = 0.3\lambda_m$, the cutoff of the lowest-order bound mode (ω_{cf}^b) for the upper bound-mode zone is very close to the ferromagnetic resonance, leaving us a big challenge to realize one-way trapping light near the ferromagnetic resonance. In order to introduce a bandgap within $[\omega_{sp}^+, \omega_{cf}^b]$, so-called complete forbidden propagation (CFP) bandgap, we further analyze the dispersion for smaller d_2, i.e., $d_2 = 0.1\lambda_m$ and $d_2 = 0.05\lambda_m$, as shown in Figs. 2(a) and 2(b). ω_{cf}^b shifts up when d_2 is reduced, while ω_{sp}^+ remains unchanged, resulting in larger bandgap with smaller d_2. The CFP bandgap $\Delta\omega_{CFP}$ are indicated by the blue shaded rectangles. It is found that $\Delta\omega_{CFP} = 0.08\omega_m$ for $d_2 = 0.1\lambda_m$, $\Delta\omega_{CFP} = 0.5\omega_m$ for $d_2 = 0.05\lambda_m$. We emphasize that the ferromagnetic resonance frequency, as well as the COWP region (corresponding to the yellow shaded areas in Fig. 2) are independent to the thickness of YIG.

It is desired that the proposed two-dimensional (2D) one-way waveguide can be extended to a realistic three-dimensional (3D) system. For this purpose, let's terminate the 2D waveguide with a pair of metal slabs (separated by a distance of w) in the x direction, see the inset in Fig. 2(b). The formed 3D system has a finite width w in the lateral direction. Assuming that w is enough small, the 3D system can only support a fundamental mode for the frequency range of interest.

Optical Materials EXPRESS

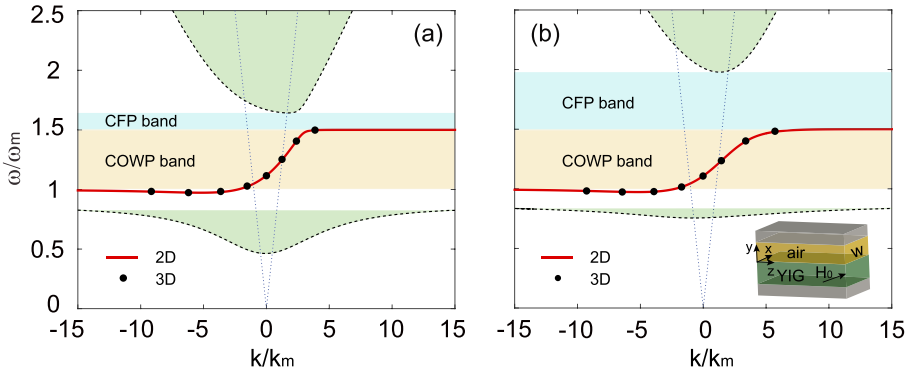

Fig. 2. Dispersion relations of guiding modes for the 2D (solid lines) and 3D (solid circles) guiding system with the case (a) $d_2 = 0.1\lambda_m$, (b) $d_2 = 0.05\lambda_m$. The blue zones represent the complete forbidden propagation (CFP) band. The inset is a 3D system corresponding to the 2D system in Fig. 1(a).

This fundamental mode is TE polarized and its fields are uniform in the x direction. Therefore, the 3D system is equivalent to the 2D system in physics, and the dispersion of the fundamental mode in the 3D system is completely identical to that in the corresponding 2D system, see Figs. 2.

The ferromagnetic resonance frequency arises from the finite YIG thickness [3]. On the other hand, there exists the plasma resonance frequency supported at the air-YIG interface. Therefore, it is interesting to investigate modal properties for the guiding mode, see the red line in Fig. 2(b), by

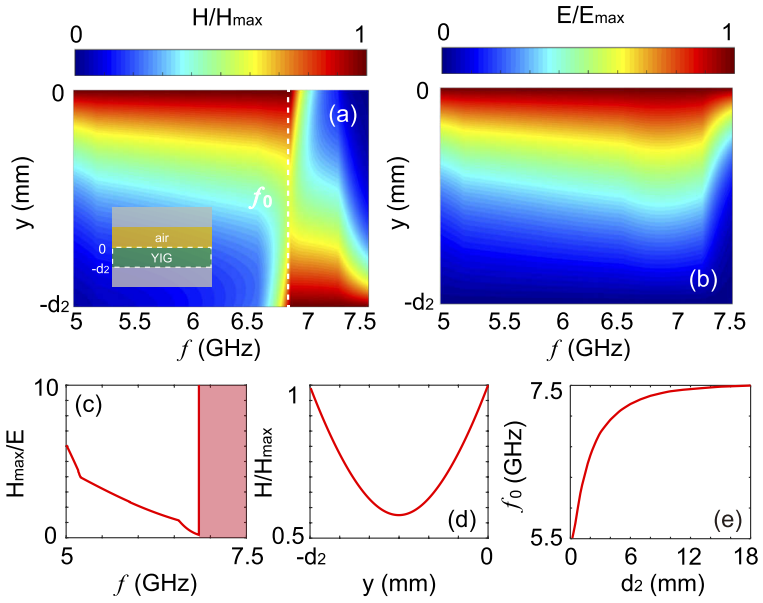

Fig. 3. Mode profile ($-d_2 \le y<0$) as a function of the working frequency for the guiding mode. (a) Magnetic field profile; (b) Electric field profile. (c) The ratio of the maxima magnetic field to the corresponding electric field as a function of the working frequency. The shaded rectangle represents the infinite value area. (d) Magnetic field profile at $f_0 = 6.83$ GHz, see the dashed line in (a), showing the transition frequency from the SMP-like to magnetostatic-like modes. (e) f_0 as a function of YIG thickness.

Optical Materials EXPRESS

checking the mode profile along the y direction in the YIG layer. Figures 3(a) and 3(b) show the mode profile ($-d_2 \leq y<0$) of the magnetic (electric) field versus frequency ranging from 5 GHz (ω_{sp}^-) to 7.5 GHz (ω_{sp}^+) for the case of $d_2 = 0.05\lambda_m$, which is normalized to the maxima magnetic (electric) field amplitude at each frequency. The mode profile of the magnetic field illustrates that the magnetic field is highest at the air-YIG interface at a lower frequency, while highest at the YIG-metal interface at a higher frequency. However, the electric field is always highest at the air-YIG interface at any frequency. Figure 3(c) shows the ratio of the maxima magnetic field to the corresponding electric field as a function of the working frequency, illustrating that the ratio has normal value at lower frequency while it is infinite at higher frequency (see the shaded area). Therefore, we conclude the guiding modes present different mode profile when changing the frequency. We refer to the guiding mode at lower frequency as SMP-like mode, while guiding mode at higher frequency as the magnetostatic-like mode. Here we introduce a threshold frequency f_0 to indicate this transition, see the vertical line in Fig. 3(a), which is defined by the factor that the amplitude of the magnetic field is the same at the air-YIG and YIG-metal interfaces, see Fig. 3(d). Moreover, the transition frequency is sensitive to the YIG thickness. We also calculate f_0 as a function of d_2, as displayed in Fig. 3(e). f_0 becomes closer to ω_{sp}^+ when the YIG layer becomes thicker.

4. Trapping magnetic rainbow by using one-way magnetostatic-like modes

For the MAYM structure, the dispersion curves should not only be sensitive to the YIG thickness, but also closely depend on H_0. Figure 4(a) shows the dispersion near ω_{sp}^+ with different H_0 values for the case $d_2 = 0.05\lambda_m$ where the material loss is not taken into account. Obviously, the dispersion curves move down with the decreasing of H_0. Each dispersion in Fig. 4(a) possesses an asymptotic frequency, where the group velocity ($v_g = d\omega/dk$) is equal to zero. The dots represent the threshold frequency f_0 at each H_0, showing that f_0 increases with H_0. Figure 4(b) shows the dependence of v_g on H_0 at different working frequencies. As an example, for a given frequency $1.5\omega_m$, one can manipulate the group velocity of the light by controlling the external magnetic field, achieving the zero group velocity when $H_0 = 0.5M_s$ (where $M_s = 1784$ G), see dashed line in Fig. 4(a). When H_0 is gradually changed along the propagation direction of the wave, we can not only control the group velocity of the wave, but also the modal properties. In our proposed system applied with the external field which gradually decreases in the propagation direction, an incident wave with a certain frequency f_c would be slowed down as it propagates forward. When $f_c<f_0$, the excited wave is assumed to be SMP-like mode, and it is gradually coupled to the magnetostatic-like mode and finally stopped at a critical point where the group velocity is reduced to zero. When $f_c>f_0$, the existed wave is the magnetostatic-like mode and it propagates forward at the metal-YIG interface until its group velocity is down to zero. Moreover, we also calculate the dependence of μ_v on H_0 at different frequency, see Fig. 4(c). The permeability of YIG material decreases with the increasing of H_0.

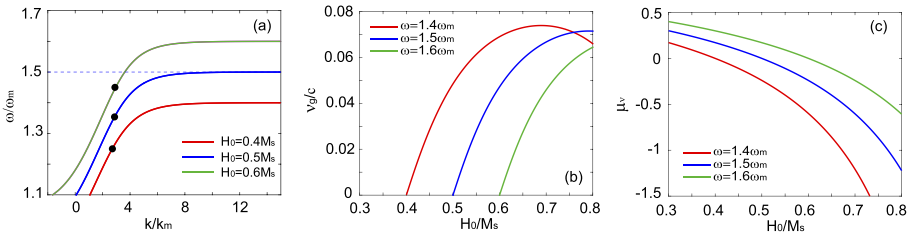

Fig. 4. (a) Dispersion relations for different external magnetic field. (b) v_g versus H_0 at three frequencies. (c) μ_v versus H_0 at three frequencies.

Optical Materials EXPRESS

We further investigate the so-called trapped rainbow effect by using of our proposed system with gradually changed external magnetic field, see Fig. 5(a). Figure 5(a) shows the 3D system with continuously decreasing H_0 over the length of 120 mm in the z direction. Because the 3D system is uniform in the x direction, the guiding modes in such a 3D system have the same properties as those in the 2D guiding system, as mentioned in part three. The continuously decreasing $H_0(z)$ is set as $H_0(z) = (0.7 - \delta z/\lambda_m)M_s$, where δ indicates the decreasing rate of $H_0(z)$ (i.e., $H_0 = 1248.8$ G when $z = 0$ mm, $H_0 = 535.2$ G when $z = 120$ mm). The parameters are chosen as follows: $d_2 = 3$ mm (i.e., $d_2 = 0.05\lambda_m$), $\delta = 0.2$, $\nu = 0.001$. We firstly investigate the rainbow effect in our system with the aid of commercially available solver in frequency domain (COMSOL Multiphysics). A TE_{01} mode at $z = 0$ mm is launched at three different frequencies of 7 GHz, 7.5 GHz and 8 GHz (corresponding to $1.4\omega_m$, $1.5\omega_m$ and $1.6\omega_m$), and the corresponding magnetic field amplitudes are plotted in Figs. 5(b-d). As expected, the one-way propagating waves with three frequencies are all stopped and hotspots with enhanced magnetic fields occur at different positions, which is consistent to the discussion mentioned above with respect to the slow light with varying the external magnetic field. Figure 5(e) show the distributions of normalized H field amplitude ($\bar{H}$) along the YIG-metal interface for the three cases, which are normalized to the values at $z = 0$ mm. It clearly indicates that the magnetic hotspot presents at $z = 90$ mm for $f = 7$ GHz, $z = 60$ mm for $f = 7.5$ GHz, and $z = 30$ mm for $f = 8$ GHz. The magnetic enhancement is 113 times for $f = 7$ GHz, 76 times for $f = 7.5$ GHz and 45 times for $f = 8$ GHz. Different from the previous works for the trapped rainbow effect, our system obtains strong magnetic field enhancement rather than electric field enhancement mentioned in Refs. ([14–18,28]). The field

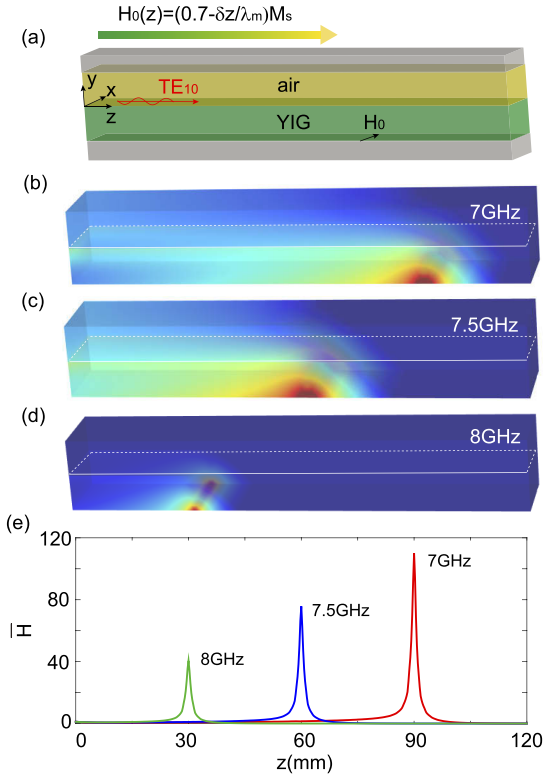

Fig. 5. (a) Schematic of our proposed configuration applied with variable H_0. Simulated H field at different frequencies, (b) 7 GHz, (c) 7.5 GHz, (d) 8 GHz. (e) Distributions of H field amplitude along the YIG-metal interface at different time.

Optical Materials EXPRESS

enhancement corresponds to the accumulation of magnetostatic-like energy which occurs at the metal surface. For the case of TE mode, the electric field has only one component tangential to the interface, which is extremely small, therefore the enhanced energy density must be related to "magnetic" charges rather than electric charges. The magnetic field of the trapped wave has a nonzero component normal to the interface, so the "magnetic" charges can be effectively heaped, resulting in magnetic field enhancement.

The frequency-domain results calculated by COMSOL are actually steady-state solutions, and it is also necessary to employ time-domain evolution to clarify the trapping process with time going on. To illustrate this, we trace the time evolution with our recently developed finite-difference time-domain (FDTD) method, which is carefully described in our previous work [24]. In the simulation, a superimposed Gaussian pulse of linear electric current is introduced as microwave source. The source is placed at $z = 0$ mm. The continuous decreasing of H_0 is the same as that mentioned in the frequency-domain investigation. The linear electric current varies with time as $F \cdot exp(-(t - t_0)^2 - \tau^2))$ $(t \geqslant 0)$, where $\tau = 32T_0$, $t_0 = 50T_0$ $(T_0 = 2\pi/\omega_m)$, and $F = F_1 + F_2 + F_3 = exp(-i2\pi f_{c1}t) + exp(-i2\pi f_{c2}t) + exp(-i2\pi f_{c3}t), f_{c1} = 8$ GHz, $f_{c2} = 7.5$ GHz, $f_{c3} = 7$ GHz. The other parameters are as follows: $d_2 = 3$ mm and $\nu = 0.001$.

The evolution of simulated magnetic field amplitudes with time is displayed in Figs. 6(a)-(d). At the beginning of the evolution, e.g., $t = 8T_0$, the wave packet almost consists of SMP-like mode and it is mainly confined at the air-YIG interface. As the evolution time goes on, due to the one-way feature, the wave packet only travels forward and is hybridized by the SMP-like mode at the air-YIG interface and the magnetostatic-like mode at the YIG-metal interface, as shown in Figs. 6(b) and 6(c). When the wave packet continuously travels, the wave packet consists of the magnetostatic-like mode sustained at the YIG-metal interface and finally stops when $t = 60T_0$, as shown in Fig. 6(d). The hotspots with extremely strong magnetic field are generated near

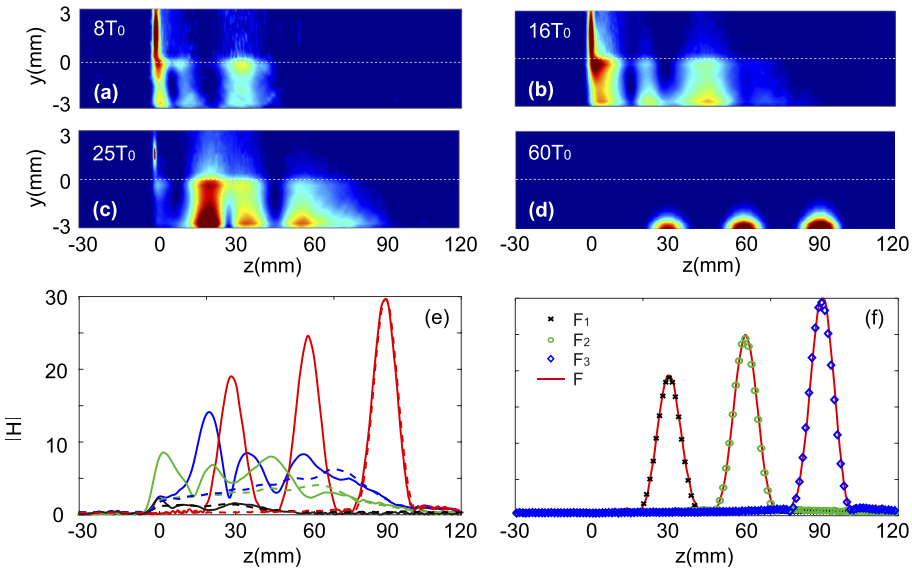

Fig. 6. FDTD simulated H amplitudes at different evolution times: (a) $8T_0$, (b) $16T_0$, (c) $25T_0$, (d) $60T_0$. (e) Distributions of H field amplitude along the YIG-metal interface. The solid lines and dashed lines represent the distributions of H for the three-frequency time-pulse system and the single lowest frequency time pulse, respectively. The external magnetic field is set as $H_0(z) = (0.7 - \delta z/\lambda_m)M_s$. (f) Distributions of H field amplitude along the YIG-metal interface at $t = 60T$ for three separate Gaussian pulses.

Optical Materials EXPRESS

the YIG-metal interface, which are consistent with those obtained by the frequency-domain simulations. In addition, the time-domain simulation gives us a clear view about how the SMP-like mode transforms to the magnetostatic-like mode when H_0 gradually decreases in the propagation direction. Figure 6(e) shows the distributions of the magnetic field amplitude ($|H|$) at the YIG-metal interface, along the z axis at different evolution time. The solid lines and dashed lines in Fig. 6(e) represent the distributions of $|H|$ for the three-frequency time-pulse system and the single lowest frequency time pulse, respectively. With the evolution of the time, the magnetic field is significantly enhanced at the YIG-metal interface ($y = -3$ mm). Figure 6(f) shows $|H|$ along the YIG-metal interface at $t = 60T$ for three systems where the center frequencies of the Gaussian pulses are set as f_{c1}, f_{c2} and f_{c3}, respectively. For comparison, the corresponding $|H|$ at $t = 60T$ in Fig. 6(e) for the system with superimposed Gaussian pulse is also plotted as solid line. $|H|$ have the same values in the system with superimposed Gaussian pulse as that in three separate systems with one center frequency.

5. Conclusion

In summary, we have investigated the trapped magnetic rainbow effect in the MAYM system under a continuously decreasing external magnetic field along the wave propagation direction. The dispersion for various YIG thicknesses in the MAYM system under a static external magnetic field H_0 have been analyzed, showing that our systems provide a COWP bandgap, CFP bandgap and ferromagnetic resonance frequency. The modal properties have also been investigated, presenting a transition from the SMP-like mode to magnetostatic-like mode. The group velocities and modal properties of the waves can be manipulated by a continuously decreasing H_0 along propagation direction of the wave, i.e., waves can be transformed from the SMP-like to magnetostatic-like mode and finally stopped. The trapped magnetic rainbow effect as well as magnetic hotspots have been observed in both frequency- and time-domain. Compared to the previous works for trapping rainbow, the present system not only has the one-way feature, but also shows the trapped magnetic rainbow effect. The trapping rainbow with strong magnetic field enhancement could be used for applications in magnetic sensing and magnetic non-linearity.

Funding

National Natural Science Foundation of China (41331070, 61372005); Danish Council for Independent Research (9041-00333B).

Acknowledgments

Q.S. conceived the idea of this work. Q.S. and L.F.S. performed the simulations. W.D.M. and J.X. helped with the theory. C.H.W. and X.H.D. helped with the modeling and simulations. S.S.X. and Q.S. wrote the manuscript. All authors reviewed the manuscript.

Disclosures

The authors declare that there are no conflicts of interest related to this article.

References

1. R. W. Damon and J. R. Eshbach, "Magnetostatic Modes of a Ferromagnetic Slab," J. Appl. Phys. **31**(5), S104–S105 (1960).
2. P. Young, "Effect of boundary conditions on the propagation of surface magnetostatic waves in a transversely magnetised thin y.i.g. slab," Electron. Lett. **5**(18), 429 (1969).
3. T. J. Gerson, "Surface electromagnetic modes of a ferrite slab," IEEE Trans. Microwave Theory Tech. **22**(8), 757–763 (1974).
4. S. R. Seshadri, "Surface Magnetostatic Modes of a Ferrite Slab," Proc. IEEE **58**(3), 506–507 (1970).
5. H. J. Khozondar, Z. I. Sahhar, and M. M. Shabat, "Electromagnetic surface waves of a ferrite slab bounded by metamaterials," AEU-Int. J. Electron. **64**(11), 1063–1067 (2010).

Optical Materials EXPRESS

6. L. Kang, Q. Zhao, H. Zhao, and J. Zhou, "Magnetically tunable negative permeability metamaterial composed by split ring resonators and ferrite rods," Opt. Express **16**(12), 8825 (2008).
7. A. D. Fisher, "Optical signal processing with magnetostatic waves," Circuits, Syst. & Signal Process **4**(1-2), 265–284 (1985).
8. J. Han, A. Lakhtakia, and C. W. Qiu, "Terahertz metamaterials with semiconductor split-ring resonators for magnetostatic tunability," Opt. Express **16**(19), 14390–14396 (2008).
9. A. I. Chernov, M. A. Kozhaev, I. V. Savochkin, D. V. Dodonov, P. M. Vetoshko, and A. K. Zvezdin, "Optical excitation of spin waves in epitaxial iron garnet films: mssw vs bvmsw," Opt. Lett. **42**(2), 279–282 (2017).
10. K. Okubo, V. Priye, and M. Tsutsumi, "A new magnetostatic wave delay line using yig film," IEEE Trans. Magn. **33**(3), 2338–2341 (1997).
11. T. Baba, "Slow light in photonic crystals," Nat. Photonics **2**(8), 465–473 (2008).
12. B. Corcoran, C. Monat, M. Pelusi, C. Grillet, T. P. White, L. O. Faolain, T. F. Krauss, B. J. Eggleton, and D. J. Moss, "Optical signal processing on a silicon chip at 640Gb/s using slow-light," Opt. Express **18**(8), 7770–7781 (2010).
13. Y. Cui, K. H. Fung, J. Xu, H. Ma, and Y. Jin, "Ultrabroadband Light Absorption by a Sawtooth Anisotropic Metamaterial Slab," Nano Lett. **12**(3), 1443–1447 (2012).
14. M. I. Stockman, "Nanofocusing of Optical Energy in Tapered Plasmonic Waveguides," Phys. Rev. Lett. **93**(13), 137404 (2004).
15. Z. X. Xu, J. Shi, R. J. Davis, X. X. Yin, and D. F. Sievenpiper, "Rainbow Trapping with Long Oscillation Lifetimes in Gradient Magnetoinductive Metasurfaces," Phys. Rev. Appl. **12**(2), 024043 (2019).
16. K. L. Tsakmakidis, A. D. Boardman, and O. Hess, "Trapped rainbow storage of light in metamaterials," Nature **450**(7168), 397–401 (2007).
17. H. Hu, D. Ji, X. Zeng, K. Liu, and Q. Gan, "Rainbow Trapping in Hyperbolic Metamaterial Waveguide," Sci. Rep. **3**(1), 1249 (2013).
18. B. Li, Y. He, and S. He, "Investigation of light trapping effect in hyperbolic metamaterial slow-light waveguides," Appl. Phys. Express **8**(8), 082601 (2015).
19. C. Ouyang, D. Han, F. Zhao, X. Hu, X. Liu, and J. Zi, "Wideband trapping of light by edge states in honeycomb photonic crystals," J. Phys.: Condens. Matter **24**(49), 492203 (2012).
20. Q. Gan, Y. Ding, and F. Bartoli, "Rainbow Trapping and Releasing at Telecommunication Wavelengths," Phys. Rev. Lett. **102**(5), 056801 (2009).
21. J. He, Y. Jin, Z. Hong, and S. He, "Slow light in a dielectric waveguide with negative-refractive-index photonic crystal cladding," Opt. Express **16**(15), 11077–11082 (2008).
22. L. F. Shen, Z. Y. Wang, X. H. Deng, J. J. Wu, and T. J. Yang, "Complete trapping of electromagnetic radiation using surface magnetoplasmons," Opt. Lett. **40**(8), 1853–1856 (2015).
23. L. F. Shen, X. D. Zheng, and X. H. Deng, "Stopping terahertz radiation without backscattering over a broad band," Opt. Express **23**(9), 11790 (2015).
24. Q. Shen, L. J. Hong, X. H. Deng, and L. F. Shen, "Completely stopping microwaves with extremely enhanced magnetic fields," Sci. Rep. **8**(1), 15811 (2018).
25. Q. Y. Mu, F. Fan, S. Chen, S. Xu, C. Z. Xiong, X. Zhang, X. H. Wang, and S. J. Chang, "Tunable magneto-optical polarization device for terahertz waves based on insb and its plasmonic structure," Photonics Res. **7**(3), 325–331 (2019).
26. F. Fan, S. Chen, and S. J. Chang, "A review of magneto-optical microstructure devices at terahertz frequencies," IEEE J. Sel. Top. Quantum Electron. **23**(4), 1–11 (2017).
27. F. Fan, S. Chen, X. H. Wang, and S. J. Chang, "Tunable nonreciprocal terahertz transmission and enhancement based on metal/magneto-optic plasmonic lens," Opt. Express **21**(7), 8614–8621 (2013).
28. K. X. Liu and S. L. He, "Truly trapped rainbow by utilizing nonreciprocal waveguides," Sci. Rep. **6**(1), 30206 (2016).
29. J. R. Maze, P. L. Stanwix, J. S. Hodges, S. Hong, J. M. Taylor, P. Cappellaro, L. Jiang, M. V. Gurudev Dutt, E. Togan, A. S. Zibrov, A. Yacoby, R. L. Walsworth, and M. D. Lukin, "Nanoscale magnetic sensing with an individual electronic spin in diamond," Nature **455**(7213), 644–647 (2008).
30. X. Yao and A. Belyanin, "Giant Optical Nonlinearity of Graphene in a Strong Magnetic Field," Phys. Rev. Lett. **108**(25), 255503 (2012).
31. J. Chen, T. Zha, T. Zhang, C. Tang, Y. Yu, Y. Liu, and L. Zhang, "Enhanced Magnetic Fields at Optical Frequency by Diffraction Coupling of Magnetic Resonances in Lifted Metamaterials," J. Lightwave Technol. **35**(1), 71–74 (2017).
32. X. Deng, L. Hong, X. Zheng, and L. Shen, "One-way regular electromagnetic mode immune to backscattering," Appl. Opt. **54**(14), 4608–4612 (2015).
33. A. W. Snyder and J. D. Love, *Optical Waveguide Theory* (Chapman and Hall, 1983).